

000 OOWL500: Overcoming Dataset Collection Bias 001 in the Wild

002
003 Brandon Leung, Chih-Hui Ho, Amir Persekian, David Orozco, Yen Chang,
004 Erik Sandstrom, Bo Liu, Nuno Vasconcelos
005
006

007 UC San Diego
008 {b7leung, chh279, aperseki, dorozco, yec084, esandstr, boliu,
009 nvasconcelos}@ucsd.edu
010
011

012 **Abstract.** The hypothesis that image datasets gathered online “in the
013 wild” can produce biased object recognizers, e.g. preferring professional
014 photography or certain viewing angles, is studied. A new “in the lab”
015 data collection infrastructure is proposed consisting of a drone which
016 captures images as it circles around objects. Crucially, the control pro-
017 vided by this setup and the natural camera shake inherent to flight mit-
018 igate many biases. It’s inexpensive and easily replicable nature may also
019 potentially lead to a scalable data collection effort by the vision commu-
020 nity. The procedure’s usefulness is demonstrated by creating a dataset of
021 *Objects Obtained With fLight* (OOWL). Denoted as OOWL500, it con-
022 tains 120,000 images of 500 objects and is the largest “in the lab” image
023 dataset available when both number of classes and objects per class are
024 considered. Furthermore, it has enabled several of new insights on ob-
025 ject recognition. First, a novel adversarial attack strategy is proposed,
026 where image perturbations are defined in terms of semantic properties
027 such as camera shake and pose. Indeed, experiments have shown that
028 ImageNet has considerable amounts of pose and professional photogra-
029 phy bias. Second, it is used to show that the augmentation of in the wild
030 datasets, such as ImageNet, with in the lab data, such as OOWL500,
031 can significantly decrease these biases, leading to object recognizers of
032 improved generalization. Third, the dataset is used to study questions
033 on “best procedures” for dataset collection. It is revealed that data aug-
034 mentation with synthetic images does not suffice to eliminate in the wild
035 datasets biases, and that camera shake and pose diversity play a more
036 important role in object recognition robustness than previously thought.

037
038 **Keywords:** Pose dataset; Large-scale image dataset; Deep learning; Im-
039 age classification; Object recognition
040
041

042 1 Introduction

043 The last few years have shown that large convolutional neural networks (CNNs),
044 such as Alexnet [1], VGG [2], GoogleNet [3], ResNet [4], etc. achieve previously
045 unmatched object recognition performance. It is also well established that these
046 models can be easily transferred to other tasks by fine-tuning. As a result, CNNs
047 are now almost universally used in computer vision. Many variants on object



Fig. 1: Results of a Google image query for *dogs from behind*.

recognition architectures have also been proposed for object detection [5–7], action recognition [8, 9], image captioning [10], question answering [11], etc. In summary, object recognition breakthroughs have had a surprisingly large “multiplier effect” for the whole of computer vision.

Besides CNNs, much of this progress can be ascribed to the introduction of ImageNet [12]. With 1 million images covering 1,000 object classes, it is one of the largest datasets in the literature. Additionally, the ease with which ImageNet trained networks can be transferred to other tasks suggests that it enables the learning of *universal visual representations*. It could be argued that, at least for lower convolutional layers of modern CNNs, filters learned on ImageNet are applicable to most vision tasks. While fine-tuning on specific data may enable gains, these are usually marginal. In many cases, the simple use of ImageNet CNNs as “feature extractors” is a strong baseline. All of this suggests that ImageNet experiments enable fundamental conclusions about object recognition. For example, because modern CNNs achieve smaller error than human annotators on ImageNet, it has been claimed, both in technical [13–15] and popular [16–18] literature, that CNNs have superhuman object recognition performance.

Nevertheless, experience has shown that most datasets have biases [19]. Like many recent vision datasets, ImageNet is the product of data collection “in the wild” – images are first collected on the internet, then annotated on platforms like MTurk. Dataset collection in the wild is a major departure from classic vision practice of collection “in the lab”. Its main advantage is removing dataset biases ensuing from a limited number of object classes, objects per class, lighting patterns, backgrounds, imaging systems, etc. However, there are at least two significant limitations. First, images collected on the web have some biases of their own. This is because people who upload do a certain amount of self selection, usually seeking to publish “good” images. Consequently, it is not easy to collect large quantities of images of objects in the wild under *unpopular imaging settings*, such as “poor” lighting, “uncommon” or “improper” object views, “poor” focus, motion blur, etc. These unpopular settings vary with the object class. While trees are photographed from all angles and distances, dog pictures tend to depict close-ups of dog faces. Fig. 1 illustrates this point by showing a set of images returned by Google image search for the query “*dogs from behind*”. This makes it likely that object recognizers learned in the wild will have much more difficulty recognizing dogs from behind than frontally.

A second important limitation is that the lack of explicit control over the imaging process makes difficult to determine ImageNet’s biases. In fact, because

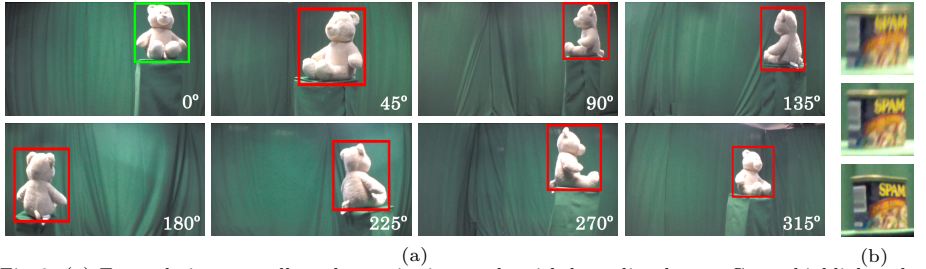


Fig. 2: (a) Example images collected per viewing angle with bounding boxes. Green highlights the frontal view. (b) Examples of varying levels of focus captured while hovering.

the images used to evaluate performance are also collected in the wild, this can be impossible. A lack of “dogs from behind” in the test set makes it impossible to know if a recognizer fails on such images. Even when the biases can be observed, it is nearly impossible to quantify them. Since Turkers are poor estimators of variables such as object viewing angle (which we denote as *pose*), lighting angle, etc., it is difficult to recover these annotations a posteriori. This hampers research in topics such as pose-invariant or light-invariant object recognition. We believe that progress along these directions requires bringing dataset collection back “to the lab” and enabling explicit control over variables such as object pose, distance, or lighting direction. Several previous works have addressed these problems [20–22]. However, many of these efforts predate deep learning, aiming for datasets much smaller and less diverse than what is expected today. Camera domes or turntables were favored, which can be expensive and cumbersome to build and maintain. We believe that more scalable data collection procedures, which can quickly be disseminated and replicated throughout the vision community, are needed to address today’s requirements.

In this work, we address this problem by proposing a new solution to scalable dataset collection “in the lab”. This leverages the fact that drones are becoming ubiquitous, cheap, and easy to program, allowing the collection of controlled object datasets to be scaled up. We consider the problem of pose invariant recognition, and propose a drone based setup to collect images over a set of object views. As illustrated in Fig. 3 this consists of having a drone fly around the object and collecting pictures at precise pose intervals. The inexpensive drone selected is commercially available, and the setup only requires tape and software. Hence, it can be easily replicated or scaled to different environments. Since all code will be made publicly available, we believe that it could enable a community wide effort on in the lab data collection. This is not easy with turntables or camera domes, which are more expensive and substantially harder to build and maintain. We also demonstrate the feasibility of the proposed setup by introducing a new dataset of *Objects Obtained With fFlight* (OWL). Denoted OOWL500, it contains 120,000 images of 500 different objects, imaged from 8 viewing angles. The images are labeled for both identity

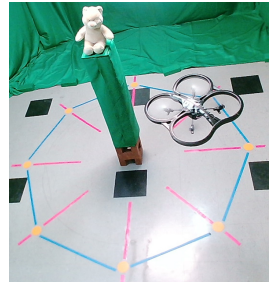


Fig. 3: The proposed drone based data collection setup.

(object and object class), pose, and other metadata that facilitates a number of experiments discussed in the paper.

OWL500 has several unique properties compared to past pose datasets. First, it is larger in regards to its combination of number of classes and number of object instances per class. Second, unlike datasets collected with domes or turntables, there is a small “camera shake” effect that produces images with statistics different than those of ImageNet style datasets. While still perfectly recognizable to humans, motion blur and somewhat lower resolutions pose additional difficulties to ImageNet trained classifiers, beyond the lack of pose robustness. This is an effect similar to adversarial attacks that are now commonly studied in the literature [23, 24]. Hence, OOWL500 is a stronger challenge for ImageNet classifiers than previous pose datasets. Third, OOWL500 has larger class overlaps with ImageNet than previous datasets and was designed to additionally overlap with a synthetic pose dataset, ModelNet [25]. All of this enables several experiments that were not possible with previous datasets.

We leverage all these properties to investigate numerous questions regarding the robustness of current object recognizers. A number of surprising observations ensue from these experiments. These include the fact that ImageNet classifiers have far weaker generalization than humans, that it is quite easy to mount adversarial attacks on current classifiers by simply manipulating object pose, that pose diversity is as important as instance diversity for training object recognizers, that synthetic data is not very helpful in mitigating the limitations of datasets collected in the wild, and that the augmentation of ImageNet with OOWL500 style images leads to more robust recognition. While some of these conclusions are not qualitatively surprising, the *strength* of the effects, i.e. the gains or losses in recognition accuracy, can be surprisingly large. This shows that much more research is needed in object recognition methods with good generalization across poses and higher robustness in general. We thus believe that the combination of our experimental observations, and the introduction of OOWL500, will inspire substantial further research in this area.

2 The OOWL500 dataset

In this section, we present the proposed drone-based setup for image collection “in the lab” and the resulting OOWL500 dataset.

2.1 Dataset collection setup

Fig. 3 shows the proposed setup for image collection “in the lab”. A drone flies around an object, following flight commands issued by a state machine implemented in software which relies on colored markings on the floor for navigation. The drone always takes off from the same 3D location and stops at orange circles on the ground. At these locations, it faces the object to take pictures at particular viewing angles, producing the images shown in Fig. 2(a). The enclosure and the platform used to place objects upon are surrounded entirely by green screens, preventing recognition algorithms from exploiting background cues. Since the objects are ultimately cropped, using the bounding boxes shown in Fig. 2(a), there are no strong background effects.

The flight space is illuminated by six LED lamps attached to the ceiling, ensuring approximately homogeneous illumination of the object under all views. As shown in Fig. 2(a), there can still be lighting variations on the object surface. This is due to surface curvature or other properties, not the existence of a preferred light direction. To prevent object recognition algorithms from exploiting lighting patterns to ascertain pose, the placement of objects' front face was randomized in regards to which wall it faced. The procedure used to control the drone flight is facilitated by its two cameras. One faces the ground, and is used for navigation. The second faces the object, and is used to collect object views. Images collected by the ground facing camera are processed by standard OpenCV vision operators to detect the floor markings. As the drone approaches the object, a PID controller issues commands to adjust its altitude, center the orange circle in the ground view, and rotate towards the pink line's direction. Once in place, the drone hovers and takes 30 pictures using the frontal camera at a rate of 5 Hz. At this point, the drone uses the ground camera to follow the blue line to the next orange circle. This sequence of commands loops until the drone finishes flying around the object. The software is implemented so that new states can easily be programmed and inserted into the sequence in any order, allowing for many potential flight configurations.

Crucially, no further intervention is needed once the drone has been placed on the first stop. A single button press instructs the drone to calibrate, take off, fly around the object, save images, and land autonomously in about 5 minutes. A video of a typical flight is provided as supplemental material, and precise details about the setup as well as all code will be released upon publication of the paper. This will make the infrastructure easily reusable, as a black box, by anyone who intends to generate a dataset or augment OOWL500. Furthermore, the code is written to accommodate flight paths of any reasonable size and shape, as indicated by the floor markings. Because only a laptop, a drone, and colored tape suffice to capture objects of many different sizes within a wide range of backgrounds and lighting conditions, we hope that these factors will result in a community wide effort to generate a very large dataset.

Another interesting facet that we plan to explore in the future is that although this is an “in the lab” setup, it can actually be deployed outside the lab. This raises the possibility of a mixed “in the lab” and “in the wild” setting, where the procedure is deployed outdoors against natural backgrounds but retains the ability to control variables like pose and distance to the object. The setup can even be scaled up to very large objects such as entire buildings or monuments. Currently, the choice to optimize the setup for low-end drones prevents us from doing this. We have so far used a Parrot A.R. Drone quadcopter because, at a cost of about \$200, it comes equipped with an ultrasound altimeter, an accelerometer, a gyroscope, and two (forward and bottom facing) cameras used to facilitate data collection. This was primarily motivated by the desire of a very low barrier to entry for those interested in contributing to dataset collection. This is unlike most previous “in the lab” image collection procedures, based on turntables or domes, that are much more expensive and difficult to build.

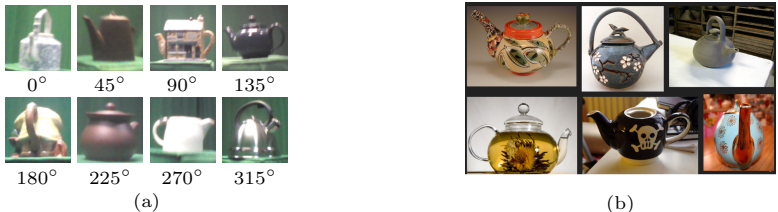


Fig. 4: Images from the “teapot” object class. Left: OOWL500. Right: ImageNet.

However, the current drone can be challenging to control outdoors. We plan to support other drones in the future.

2.2 Dataset

The above setup was used to create the OOWL500 dataset, which contains 500 objects captured at varying angles, for a total of 120,000 images. The objects are evenly distributed among 25 classes of everyday objects, such as backpacks, bottles, shoes, and teddy bears. To facilitate the experiments in Section 3, these classes have been chosen to maximize overlap with those of ImageNet [12] and ModelNet [25]. There are 20 objects per class, imaged from the 8 views (poses) of Fig. 3. Since 30 images are taken per view, each object originates 240 images, for a total of 120,000 images. As shown in Fig. 2(a), views are acquired in steps of 45°. The 240 pictures are stored as 640 × 360 PNGs.

Besides the richness of poses, OOWL500 has an adversarial aspect for classifiers trained on previous datasets, due to the somewhat unorthodox nature of images collected by the drone. While several pictures portray the same object at the same pose, they vary in object position, blurriness, exposure, and noise. Shown in Fig. 2(b), this is due to camera shake that ensues as the drone hovers in place. Some images in the “teapot” class are shown in Fig. 4(a). Note the different “feel” of these images vs. teapot examples from ImageNet, shown in Fig. 4(b). The latter illustrate an ImageNet bias towards “professional quality” object shots, which results from the “self-selection” usually performed for images posted on the web. The camera shake effect of OOWL500 can be thought as a generalization of the standard manipulations, such as pixel-swapping, commonly used in adversarial attacks to CNNs [23, 24] or image shifting and rescaling commonly used to augment training sets. The variation due to hovering naturally generates images for either attacking existing networks or augmenting training sets to build better ones. This trait is explored further in Section 3.2.

Each image in the dataset is accompanied by a CSV file that provides the following annotated information regarding the object: a short description; the pose in degrees relative to other pictures of that object; whether or not the picture depicts the object’s frontal face (denoted by a 1 or 0 respectively, or a -1 if the object does not have an easily identifiable front face); the object’s degree of rotational symmetry (indicated by the next degree increment where the object appears identical); and coordinate pairs specifying the bounding box.

Dataset	Domain	Classes	Objects per cls	Images per obj	Total Images	Overlap ImageNet	Overlap OOWL
In the wild							
Caltech-101 [26]	General	102	90	1	9,144	7	
Pascal [27]	General	20	790-10,129	1	11,540	5	
Caltech-256 [28]	General	257	119	1	30,607	17	
MNIST [29]	Digit	10	6,000	1	60,000	0	
CIFAR-100 [30]	General	100	600	1	60,000	9	
MS COCO [31]	General	80	~11,079	1	123,287	17	
ImageNet [12]	General	21,841	~650	1	14,197,122	23	
In the lab							
Table-Top-Pose [32]	Table Top	3	10	~16	480	2	1
NYC3DCars [33]	Car	1	3,787	1	1,287	1	1
EPFL Car [34]	Car	1	20	~115	2,299	1	1
ETH-80 [35]	General	8	10	41	3,280	4	1
Multi-PIE [36]	Face	1	337	15	5,055	0	0
COIL [20]	General	100	1	72	7,200	-	-
FERET [37]	Face	1	1199	1-24	14,051	0	0
PASCAL 3D+ [38]	General	12	~1158	~3	30,899	10	6
NORB [22]	Toy	5	10	1944	48,600	1	3
T-LESS [39]	Industry	30	1	648-1,296	~49,000	0	0
ALOI [21]	General	1000	1	72	72,000	-	15
iLab-20M [40]	Toy Vehicle	15	25-160	1,320	21,798,480	11	4
HIM [41]	General	51	~6	~750	250,000	19	7
OWL500	General	25	20	240	120,000	23	-
Synthetic							
ModelNet [25]	General	40	100	3D	3D	28	10
ShapeNet-55 [42]	General	55	~940	3D	3D	46	16

Table 1: Overview of well known object recognition datasets. For datasets with pose annotations, the number of overlapped classes with ILSVRC2012 are listed. This is not applicable for COIL and ALOI however (only individual objects are provided instead of classes).

2.3 Relation to previous datasets

In the wild datasets Table 1 compares OWL500 to previous datasets. The top third of the table summarizes the properties of “in the wild” datasets. These will continue to have a critical role in object recognition; they cover a diversity of imaging scenarios, objects, scenes, and scene configurations not replicable in the lab. They are listed mostly for calibration of what constitutes a large object recognition dataset today. Note that, with less than 30,000 images, Pascal and the two Caltech datasets are now considered “small” in comparison to MS-COCO and ImageNet. At 60,000 images, MNIST and CIFAR are still widely used in machine learning, but less so in computer vision. This suggests a threshold of 60,000 images, marked by the horizontal lines in the table.

The goal of this work is not to replace in the wild datasets. Rather, we seek to complement them by investigating two of their limitations. The first is that they exhibit some *biases* resulting from image collection on the web. One example is the *professional photography* bias of Fig. 4(b). Since most people post images to convey a message, they often carefully self-select the images to post. Hence, objects can have “standardized poses” that makes them more easily recognizable or appealing. This helps explain the *pose bias* of Fig. 1. This bias is also visible on the ImageNet teapots of Fig. 4(b), which tend to be presented from a side view. The second limitation of “in the wild” datasets is the lack of information needed to study important questions in object recognition, such as invariance to pose, scale, lighting, etc. Consider pose variability. Under mild assumptions on imaging setup (e.g. uniform lighting), a rigid object spans a 3D manifold in

image space as the viewing angle changes. This suggests a decomposition into the *appearance* and the *pose* information of the object. An object recognizer could, in principle, exploit this decomposition to improve its generalization, e.g. by leveraging a model of pose trajectories learned from some objects to better recognize others, for which less training views are available. This is easier if the dataset contains *pose trajectories*, i.e. multiple views of each object, and even more likely if the dataset is annotated with *pose labels*. None of the two hold for “in the wild” datasets, which favor instance diversity. For example, ImageNet contains 1,000 images of chairs but no different views of the same chair. Even if this were the case, pose labels would be difficult to recover on MTurk.

In the lab datasets The study of these questions has motivated several “in the lab” datasets, annotated for factors like pose, distance, or lighting. In fact, as shown in the second third of Table 1, there is a long history of such datasets. However, most of them are below the 60,000 image threshold, and too small to train deep CNNs. Furthermore, they all have significant differences compared to OOWL500. First, they exhibit a professional photography bias similar to

that of in the wild datasets. Sometimes the bias is even stronger, because images are collected in a precisely controlled studio environment; they do not exhibit the camera shake found in OOWL500. Second, objects are often carefully selected from fine-grained classes, such as faces or toys. Due to this, many of these datasets have few classes of overlap with in the wild datasets like ImageNet (only HM comes close to OOWL500 in this regard). This prevents studies of robustness, such as the ones we pursue in this work, or the use of these datasets to augment ImageNet. Third, beyond total number of images, an object dataset should contain a number of classes sufficiently large to pose a challenging discrimination problem, and a number of object instances large enough to capture the diversity of appearances of each class. Even the largest in the lab datasets can be small in this respect. For example, while iLab-20M contains many images, it only includes 15 classes of toy vehicles. This is a relatively small classification challenge. On the other hand, HM contains 51 classes, but only a few objects (6 on average) per class. This is not enough to capture the appearance diversity of most object classes. Since dataset size is combinatorial on these factors, any dataset must achieve a good compromise between them. Fig. 5 visualizes this

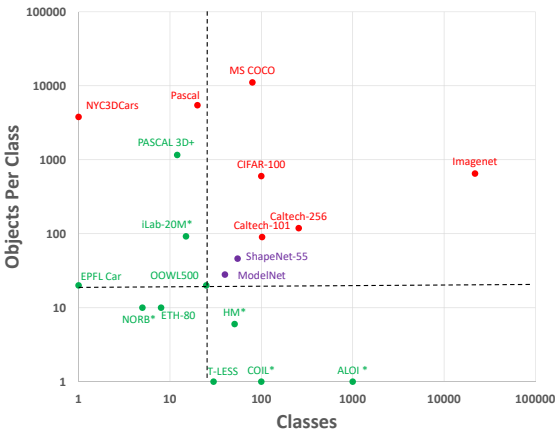


Fig. 5: Scatter plot of datasets listed in Table 1. In the wild datasets are shown in red, in the lab in green, and synthetic in purple. An asterisk indicates that turntables were used for data collection.

trade-off, by showing the number of classes vs. objects per class of each dataset in Table 1. Among in the lab datasets (shown in green), OOWL500 achieves the best trade-off between the two factors. Naturally, in the wild datasets tend to be larger in size. However, the scalability of the drone-based data collection process used by OOWL500, together with the potential for community wide collaborative collection, could push it to the red area of the plot. It is hard to see this happening with turntable or dome-based methods.

Synthetic datasets Recently, there has also been interest in large datasets of object shape. These are usually composed of synthetic images, rendered from 3D graphics models. Two popular datasets in this class, ModelNet [25] and ShapeNet [42] are listed in the bottom third of Table 1. While object views are comprehensive, Fig. 5 shows that they are not much larger than OOWL500 in terms of object classes or objects per class. Furthermore, these datasets have been primarily used for operations such as shape classification or retrieval on synthetic images. It is not clear whether they can be leveraged to improve real-world object recognition systems. We study this question in Section 3.3.

3 Experiments

In this section, we report various experiments using OOWL500.

3.1 Experimental setup

Datasets The goal of these experiments were to compare in the wild, in the lab, and synthetic datasets, represented by ImageNet, OOWL500, and ModelNet respectively. Given a 3D shape from ModelNet, 2D images were rendered as in [43]. A preliminary step was used to generate three datasets of comparable classes. Since ImageNet is more fine-grained than the others, several of its classes were merged in a larger class with the same number of images. For example, “airliner” and “warplane” were merged into an “airplane” class. The 1,300 training and 50 test images of each original class were randomly sampled (650 training, 25 test images per class) to produce a 1,300 (50) image “airplane” training (test) set. Appendix A and B present a list of the merged ImageNet sub-classes for each object class also found on OOWL500 and ModelNet, respectively. After this fusion, there was an overlap of 23 classes between ImageNet and OOWL500, and 8 between ImageNet, OOWL500, and ModelNet. To maximize the number of classes per experiment, several new datasets were created. *IN(23)* contains the ImageNet images of the 23 classes shared with OOWL500, *IN(8)* of the 8 classes shared by all 3 datasets, and *OOWL500(8)* the same for OOWL500. All experiments were performed with AlexNet [30], ResNet [4], and VGG [2]. Models pre-trained on the full ImageNet and fine-tuned on each of the IN datasets are denoted *ImageNet classifiers (INC)*. For example, *INC(23)* indicates the classifiers fine-tuned on *IN(23)*. Models fine-tuned on OOWL500 and ModelNet are denoted *OC* and *MNC* classifiers, respectively.

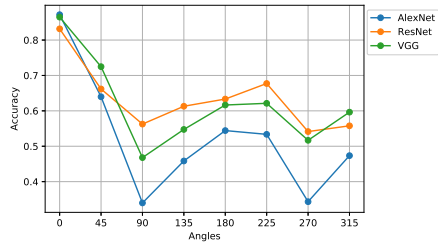


Fig. 6: Recognition rate as a function of angle perturbation $\delta\theta$. $\delta\theta = 0$ reports to camera shake, $\delta\theta > 0$ to an angle change of $\delta\theta$.

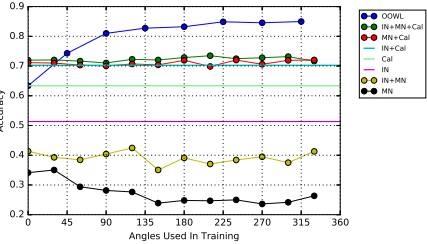


Fig. 7: Test set accuracy, on OOWL500, of classifiers trained on 8 training sets, as a function of the pose angles included in the training set.

Frontal Pose Comparing recognition accuracy as a function of pose requires a pose reference, i.e. the 0° view or *frontal pose*. This is hard to define for classes like airplanes. The most natural frontal poses (the plane’s nose or side) are also uncommon on ImageNet, where airplanes are usually seen at 45° degrees. Because of this, INCs have different “favorite poses” for different classes, under the OOWL500 definition of frontal pose. To avoid bias towards OOWL500, we adopted a data-driven definition instead. In all experiments, *frontal pose* is the view of largest average recognition accuracy by the INC classifiers for each class.

3.2 ImageNet bias

We now report on experiments testing the usefulness of OOWL500 as a tool to 1) identify biases of “in the wild” data collection and 2) help correct them.

Adversarial attacks There has recently been much interest on adversarial attacks on CNNs [23, 24]. These consist of perturbing an image in a way that does not affect human recognition and measuring the drop of recognition accuracy by the CNN. We considered an attack strategy on the INC(23) classifiers using OOWL500 images. A random frontal pose of OOWL500, correctly classified by the CNN, was perturbed into another image of either the same or a different pose. Images of the same pose differ by camera shake (small perturbation), while those of different poses differ by view and camera shake (larger). The difference of view angles is denoted the angle perturbation $\delta\theta$. This was repeated for all classes of OOWL500. Fig. 6 shows the recognition rates of the three classifiers as a function of $\delta\theta$. The attacks are quite successful, producing a low recognition rate for most values of $\delta\theta$. They exhibit the two ImageNet biases’ effects illustrated in Fig. 4. The drop to $80 - 90\%$ recognition rate at $\delta\theta = 0$, where all perturbations are due to camera shake, is explained by the “professional photography” bias of ImageNet. The even lower recognition rates for larger $\delta\theta$ are explained by its “pose bias”. Note that the latter is particularly strong, with a performance drop larger than 50 points between frontal and least favorite pose!

Correcting ImageNet biases We next studied the usefulness of “in the lab” datasets such as OOWL500 to correct ImageNet biases. A first set of experiments investigated whether OOWL500 is a useful complement to ImageNet. These were inspired by previous claims of superhuman performance for the classification of

ImageNet object classes. While this has been shown to hold when ImageNet classifiers are evaluated on the ImageNet test set [13–15], it has not been shown how their generalization to a more adversarial set up compares to that of humans. To evaluate this, we measured the recognition accuracy of the INC(23) classifiers on IN(23) and OOWL500, and compared them to those of OOWL classifiers and human performance. Human performances were evaluated by taking the majority vote of 3 individual Turkers, asked to classify test set images from OOWL500 and ImageNet. Since all classifiers behaved similarly, we only report the average across the AlexNet, VGG, and ResNet architectures, shown in Table 2. The first striking observation is that the INC(23) classifiers performed quite poorly on OOWL500. While their performance on the IN(23) test set is only 9 points weaker than that of Turk workers, the difference on OOWL500 is 46 points! Note that the differences between OOWL500 and ImageNet pose no difficulties to humans, which have similar performance on both datasets. This demonstrates the vulnerability of ImageNet classifiers to camera shake and pose bias, the importance of datasets (such as OOWL500) that account for these factors, and the fallacy of claims of superhuman performance, even on ImageNet classes.

Note that the classifier architectures are perfectly capable of handling OOWL500. When fine-tuned on the latter, the (OC) classifiers achieve good performance on this dataset. However, there is a significant drop of accuracy on IN(23). This is a well known problem, wherein fine-tuning causes the classifier to “forget” the original dataset [44, 45]. These results show that OOWL500 is a good testing ground for future research in this area. An interesting additional observation, perhaps the most surprising of this experiment, is that the OC classifiers, fine-tuned to OOWL500, generalized better to IN(23) – 44% accuracy – than the INC(23), fine-tuned to IN(23), generalized to OOWL500 – 33%. Finally, the classifiers fine-tuned on *both* IN(23) and OOWL500 nearly matched the accuracy of the classifiers fine-tuned to each dataset. While this was expected, it shows that *complementing* ImageNet with OOWL500 has no degradation on the ImageNet domain, but can substantially increase performance beyond it.

Overall, this experiment supports several conclusions. First, claims of superhuman performance regarding deep learning classifiers trained on ImageNet are widely exaggerated. It is clear that the classifiers do not even generalize for a dataset with *the same* object classes, when the images of the latter are not collected on the web. Second, the two datasets are clearly *complimentary*. When classifiers are fine-tuned on both, overall recognition performance is far superior than when they are fine-tuned on only one. Third, the strongest transfer from OOWL500 to IN(23) rather than vice versa suggests that there is more than a simple mismatch of image statistics between the two datasets. Instead, it sug-

Classifier	Dataset		
	IN(23)	OOWL500	ALOI
INC	0.79	0.33	0.55
OC	0.44	0.77	0.71
Both	0.76	0.78	0.72
Human	0.88	0.87	-

Table 2: Average recognition accuracy of AlexNet, VGG, and ResNet classifiers fine-tunned on IN(23) (denoted INC(23)), OOWL500 (denoted OC), and both (denoted both), on the test sets of IN(23), OOWL500, and ALOI. Experiments on IN(23) and OOWL500 are based on 23 classes, while those on ALOI are based on 13 classes. Human performance was measured by majority vote among three Turk workers.

495 gests the existence of an ImageNet pose bias which hurts the ability of ImageNet
 496 classifiers to generalize to data with the pose diversity of OOWL500.

497 The last point is somewhat muddled by the fact that the classifiers (OC) fine-
 498 tuned on OOWL500 were initially pre-trained on ImageNet. Their better general-
 499 ization to IN(23) could be due to the pre-training. To test this, the performances
 500 of INC and OC were evaluated on a third dataset ALOI [21] which exhibits sig-
 501 nificant pose variability and is completely independent of IN and OOWL500.
 502 Since it shares 13 classes with IN and OOWL500, *IN*(13) and *OOWL500*(13)
 503 were created with the procedure of Section 3.1. OC(13) and IN(13) classifiers,
 504 fine-tunned on these datasets, were finally tested on ALOI. As shown in Table 2,
 505 OC(13) generalized significantly better than INC(13), achieving a gain of 16
 506 points and performance nearly identical to that of the classifier fine-tuned on
 507 both IN(13) and OOWL500. This confirms the need for in the lab datasets that,
 508 like OOWL500, enable training that specifically corrects ImageNet biases.

509 3.3 Guidelines for data collection

510 So far, we have seen that OOWL500 can be used to 1) construct adversarial at-
 511 tacks on and 2) improve generalization performance of ImageNet classifiers. The
 512 final set of experiments exploited OOWL500 to obtain data collection insights.

513 **Alternative training strategies** Computer generated synthetic datasets pro-
 514 vide a simple alternative to “in the lab” datasets. In fact, recent works use
 515 synthetic data to improve the generalization of classifiers [46] or solve problems
 516 such as shape retrieval [43, 47]. To evaluate the potential of synthetic data aug-
 517 mentation, we fine-tuned ImageNet classifiers on the combined training sets of
 518 IN(8) and MN and tested their recognition performance on OOWL500(8). To
 519 characterize sensitivity to pose, various experiments were performed. Starting
 520 from IN(8), all the images with the same pose of MN were gradually added to
 521 the fine-tuning set. The first experiment included only frontal poses, then 45°
 522 views were added, and so forth. The recognition performance was recorded after
 523 each new pose set was added and is displayed in a cumulative plot in Fig. 7.
 524 Various transfer modes were compared. Modes IN and MN are baselines using
 525 ImageNet and ModelNet fine-tuning only, respectively. Mode IN+MN used the
 526 combination of the two datasets. To minimize the difficulty of transfer due to
 527 differences in the overall statistics of OOWL500, ImageNet, and ModelNet, we
 528 also considered a few “calibrated” modes where the fine-tuning set included the
 529 frontal pose of OOWL500. Mode Cal used only this set of images, modes IN-Cal
 530 and MN-Cal combined the IN and MN sets with the calibration set respectively,
 531 and mode IN-MN-Cal used all fine-tuning modes. All these transfer modes were
 532 compared to transfer based on fine-tuning on the OOWL500 training set.

533 Several conclusions can be made. First, synthetic data does *not* help the
 534 transfer at all. MN had very poor performance, which in fact decreased as poses
 535 were added. The addition of MN to IN also decreased the performance of the
 536 latter. Second, the biggest gains came from the calibration modes. The addition
 537 of the OOWL500 frontal pose significantly improved on all the other configu-
 538 rations. While this was somewhat expected, the gain is quite significant – at

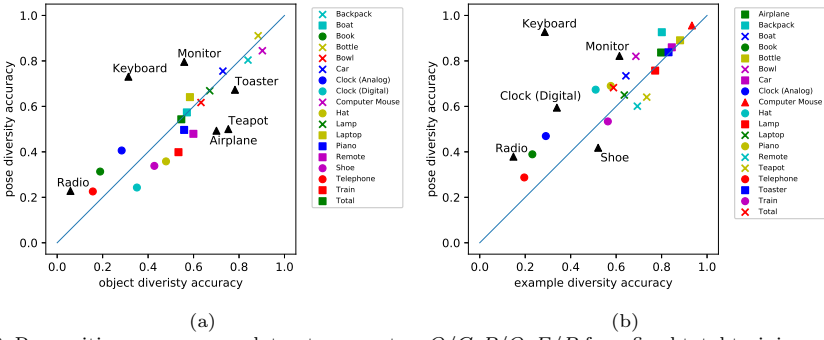


Fig. 8: Recognition accuracy vs. dataset parameters $O/C, P/O, E/P$ for a fixed total training set size (D). (a) x axis shows accuracy by training with $(O/C, P/O) = (16, 1)$, which favors object diversity; y axis by training with $(2, 8)$, favoring pose diversity. (b) x axis shows accuracy by training with $(E/P, P/O) = (30, 1)$, favoring camera shake; y axis by training with $(3, 8)$, favoring pose diversity.

least 20 points. Again, the addition of MN poses had no noticeable increase in performance. Third, the best performance was obtained with OOWL500 alone. While the addition of IN(8) and MN improved on OOWL500 fine-tuning with the frontal pose only, there were *no gains* after that. Adding a *single* pose (45°) of OOWL500 to the fine-tuning set was enough to match the performance of adding the entire IN(8) and MN training sets! Adding one further pose (90°) raised the recognition rate to a level close to the overall best. In summary, these experiments show that 1) synthetic augmentation *is not the solution* to the problem of ImageNet biases and 2) even a small number of in the lab poses guarantee major gains over the ImageNet performance.

Pose diversity vs object diversity Object recognition has many dimensions of image variability, such as the diversity of pose or appearance of the objects in each class. For a fixed dataset size, it is always necessary to establish trade-offs for the coverage of all these dimensions. In the lab datasets such as OOWL500 enable the study of how this coverage impacts the quality of the resulting classifiers. OOWL500 contains four such dimensions: the number of classes (C), the number of object instances per class (O/C), the number of poses per object (P/O), and the number of examples per pose of each object (E/P). For a fixed dataset size $D = C \times O/C \times P/O \times E/P$, many configurations of these factors are possible. For example, ImageNet uses $E/P = P/O = 1$ and favors *object diversity*, i.e. large O/C . OOWL500 enables other strategies, such as *pose diversity* (larger P/O) or *camera shake* (larger E/P). Two experiments were performed to compare the relative performance of such strategies. In both cases, we fixed the number of classes and training set size ($C = 23$ and $D = 11040$ respectively). The first experiment compared the importance of object vs. pose diversity. For this, we fixed $E/P = 30$ and considered two extreme configurations. The first, denoted *max object diversity*, used a fine-tuning set with the largest possible $O/C = 16$ and smallest $P/O = 1$. The second, denoted *max pose diversity*, used the smallest $O/C = 2$ and the largest $P/O = 8$. The recognition accuracy of classifiers trained with these fine-tuning sets was then compared.

The scatter plot of Fig. 8(a) illustrates the average recognition accuracies of the two strategies for all object classes in OOWL500. Points on the blue line signal classes with equal recognition rate under the two strategies. Points above (below) signal classes that are favored by max pose (object) diversity. Interestingly, more than half the classes have no preference or *prefer pose diversity*. While this was expected for some classes such as “Monitor” or “Keyboard,” which have relatively low object diversity but whose appearance can vary significantly with pose, it was surprising that it holds for so many. Note that most in the wild datasets only exhibit object diversity, because pose diversity is almost impossible to control in this setting. The fact that the preference for object or pose diversity varies with the class also suggests that further research is needed on intelligent data collection strategies that can take this into account. In the lab datasets, like OOWL500, enable such research.

Pose diversity vs camera shake A second experiment compared the importance of pose diversity vs. camera shake. For this, we fixed $O/C = 16$ and considered two strategies to assemble the fine-tuning set. *Max pose diversity* used $P/O = 8$ and $E/P = 3$; *max camera shake* used $P/O = 1$ and $E/P = 30$. The scatter plot in Fig. 8(b) shows the average recognition accuracies results. Points above (below) the blue line signal classes that are favored by max pose diversity (camera shake). Most classes have a clear *preference to pose diversity*, an effect even stronger than in the previous experiment. Again, while camera shake is usually simulated for (by shifting, cropping, etc.) in classifier design, pose diversity is much harder to address with in the wild datasets.

4 Conclusion

In this work, we have investigated the hypothesis that dataset collection “in the wild” is not sufficient to guarantee unbiased object recognizers. Specifically, we have argued that “professional photography” and “pose” biases are difficult to eliminate in web-based data collection and proposed a new “in the lab” data collection setup that mitigates these factors. This consists of using a drone to take images as it hovers in various spots around an object. We have shown that this setup has multiple interesting properties. First, by utilizing drone flight, it is possible to collect images of objects at controlled camera angles. This can be used to compensate pose bias. Second, the procedure is inexpensive and easily replicable. Hence, it could lead to a scalable data collection effort by the vision community. Third, drone captured images tend to have a certain amount of camera shake that mitigates professional photography bias.

The usefulness of the procedure was demonstrated through the collection of the OOWL500 dataset – the largest in the lab dataset recognition dataset in the literature when both number of classes and objects per class are considered. OOWL500 was then shown to enable a number of new insights on object recognition. First, a novel adversarial attack strategy was developed, where image perturbations are defined in terms of semantic properties such as camera shake and pose. Experiments with this strategy have shown that ImageNet indeed has

considerable amounts of pose and professional photography bias. Second, it was used to show that the augmentation of in the wild datasets, such as ImageNet, with in the lab data, such as OOWL500, can significantly decrease these biases, leading to object recognizers of improved generalization. Third, it was used to study various questions on “best procedures” for dataset collection. This has shown that data augmentation with synthetic images does not suffice to eliminate in the wild datasets biases, and that camera shake and pose diversity play a more important role in object recognizers’ robustness than previously thought.

References

1. Krizhevsky, A., Sutskever, I., Hinton, G.E.: Imagenet classification with deep convolutional neural networks. In: Advances in neural information processing systems. (2012) 1097–1105
2. Simonyan, K., Zisserman, A.: Very deep convolutional networks for large-scale image recognition. arXiv preprint arXiv:1409.1556 (2014)
3. Szegedy, C., Liu, W., Jia, Y., Sermanet, P., Reed, S., Anguelov, D., Erhan, D., Vanhoucke, V., Rabinovich, A., et al.: Going deeper with convolutions
4. He, K., Zhang, X., Ren, S., Sun, J.: Deep residual learning for image recognition. In: Proceedings of the IEEE conference on computer vision and pattern recognition. (2016) 770–778
5. Girshick, R., Donahue, J., Darrell, T., Malik, J.: Rich feature hierarchies for accurate object detection and semantic segmentation. In: Proceedings of the IEEE conference on computer vision and pattern recognition. (2014) 580–587
6. Ren, S., He, K., Girshick, R., Sun, J.: Faster r-cnn: Towards real-time object detection with region proposal networks. In: Advances in neural information processing systems. (2015) 91–99
7. He, K., Gkioxari, G., Dollár, P., Girshick, R.: Mask r-cnn. In: Computer Vision (ICCV), 2017 IEEE International Conference on, IEEE (2017) 2980–2988
8. Simonyan, K., Zisserman, A.: Two-stream convolutional networks for action recognition in videos. In: Advances in neural information processing systems. (2014) 568–576
9. Tran, D., Bourdev, L., Fergus, R., Torresani, L., Paluri, M.: Learning spatiotemporal features with 3d convolutional networks. In: Computer Vision (ICCV), 2015 IEEE International Conference on, IEEE (2015) 4489–4497
10. Karpathy, A., Fei-Fei, L.: Deep visual-semantic alignments for generating image descriptions. In: Proceedings of the IEEE conference on computer vision and pattern recognition. (2015) 3128–3137
11. Antol, S., Agrawal, A., Lu, J., Mitchell, M., Batra, D., Lawrence Zitnick, C., Parikh, D.: Vqa: Visual question answering. In: Proceedings of the IEEE International Conference on Computer Vision. (2015) 2425–2433
12. Deng, J., Dong, W., Socher, R., Li, L.J., Li, K., Fei-Fei, L.: Imagenet: A large-scale hierarchical image database. In: Computer Vision and Pattern Recognition, 2009. CVPR 2009. IEEE Conference on, IEEE (2009) 248–255
13. Rajpurkar, P., Irvin, J., Zhu, K., Yang, B., Mehta, H., Duan, T., Ding, D., Bagul, A., Langlotz, C., Shpanskaya, K., Lungren, M.P., Ng, A.Y.: Chestnet: Radiologist-level pneumonia detection on chest x-rays with deep learning. CoRR abs/1711.05225 (2017)

- 675 14. He, K., Zhang, X., Ren, S., Sun, J.: Delving deep into rectifiers: Surpassing human-
676 level performance on imagenet classification. CoRR **abs/1502.01852** (2015) 675
677 15. Shoham, Y., Perrault, R., Brynjolfsson, E., Clark, J., LeGassick, C.: Artificial 676
678 intelligence index 2017 annual report (2017) 677
679 16. Perry, T.S.: Stanford algorithm can diagnose pneumonia better than radiologists 678
680 (2017) 679
681 17. Rao, N.: Deep learning and the need for unified tools (2017) 680
682 18. Eckel, R.: Microsoft researchers algorithm sets imagenet challenge milestone (2015) 681
683 19. Torralba, A., Efros, A.A.: Unbiased look at dataset bias. In: Proceedings of the 682
684 2011 IEEE Conference on Computer Vision and Pattern Recognition. CVPR '11, 683
685 Washington, DC, USA, IEEE Computer Society (2011) 1521–1528 684
686 20. Nene, S.A., Nayar, S.K., Murase, H.: Columbia object image library (coil-100) 685
687 21. Geusebroek, J.M., Burghouts, G.J., Smeulders, A.W.: The amsterdam library of 686
688 object images. International Journal of Computer Vision **61**(1) (2005) 103–112 687
689 22. LeCun, Y., Huang, F.J., Bottou, L.: Learning methods for generic object 688
690 recognition with invariance to pose and lighting. In: Computer Vision and Pattern 689
691 Recognition, 2004. CVPR 2004. Proceedings of the 2004 IEEE Computer Society 690
692 Conference on. Volume 2., IEEE (2004) II–104 691
693 23. Papernot, N., Carlini, N., Goodfellow, I., Feinman, R., Faghri, F., Matyasko, A., 692
694 Hambardzumyan, K., Juang, Y.L., Kurakin, A., Sheatsley, R., Garg, A., Lin, 693
695 Y.C.: cleverhans v2.0.0: an adversarial machine learning library. arXiv preprint 694
696 arXiv:1610.00768 (2017) 695
697 24. Kurakin, A., Goodfellow, I., Bengio, S.: Adversarial examples in the physical world. 696
698 arXiv preprint arXiv:1607.02533 (2016) 697
699 25. Wu, Z., Song, S., Khosla, A., Yu, F., Zhang, L., Tang, X., Xiao, J.: 3d shapenets: A 698
700 deep representation for volumetric shapes. In: Proceedings of the IEEE conference 699
701 on computer vision and pattern recognition. (2015) 1912–1920 700
702 26. Fei-Fei, L., Fergus, R., Perona, P.: Learning generative visual models from few 701
703 training examples: An incremental bayesian approach tested on 101 object categories. 702
704 Computer vision and Image understanding **106**(1) (2007) 59–70 703
705 27. Everingham, M., Van Gool, L., Williams, C.K., Winn, J., Zisserman, A.: The 704
706 pascal visual object classes (voc) challenge. International journal of computer 705
707 vision **88**(2) (2010) 303–338 706
708 28. Griffin, G., Holub, A., Perona, P.: Caltech-256 object category dataset. (2007) 707
709 29. LeCun, Y., Bottou, L., Bengio, Y., Haffner, P.: Gradient-based learning applied to 708
710 document recognition. Proceedings of the IEEE **86**(11) (1998) 2278–2324 709
711 30. Krizhevsky, A.: Learning multiple layers of features from tiny images. (2009) 710
712 31. Lin, T.Y., Maire, M., Belongie, S., Hays, J., Perona, P., Ramanan, D., Dollár, P., 711
713 Zitnick, C.L.: Microsoft coco: Common objects in context. In: European conference 712
714 on computer vision, Springer (2014) 740–755 713
715 32. Sun, M., Bradski, G., Xu, B.X., Savarese, S.: Depth-encoded hough voting for 714
716 joint object detection and shape recovery. In: European Conference on Computer 715
717 Vision, Springer (2010) 658–671 716
718 33. Matzen, K., Snavely, N.: Nyc3dcars: A dataset of 3d vehicles in geographic context. 717
719 In: Computer Vision (ICCV), 2013 IEEE International Conference on, IEEE (2013) 718
720 761–768 719
721 34. Ozuysal, M., Lepetit, V., Fua, P.: Pose estimation for category specific multiview 717
722 object localization. In: Computer Vision and Pattern Recognition, 2009. CVPR 718
723 2009. IEEE Conference on, IEEE (2009) 778–785 719

- 720 35. Leibe, B., Schiele, B.: Analyzing appearance and contour based methods for object
721 categorization. In: Computer Vision and Pattern Recognition, 2003. Proceedings.
722 2003 IEEE Computer Society Conference on. Volume 2., IEEE (2003) II–409
723 36. Gross, R., Matthews, I., Cohn, J., Kanade, T., Baker, S.: Multi-pie. Image and
724 Vision Computing **28**(5) (2010) 807–813
725 37. Phillips, P.J., Moon, H., Rizvi, S.A., Rauss, P.J.: The feret evaluation methodology
726 for face-recognition algorithms. IEEE Transactions on pattern analysis and
727 machine intelligence **22**(10) (2000) 1090–1104
728 38. Xiang, Y., Mottaghi, R., Savarese, S.: Beyond pascal: A benchmark for 3d object
729 detection in the wild. In: Applications of Computer Vision (WACV), 2014 IEEE
730 Winter Conference on, IEEE (2014) 75–82
731 39. Hodan, T., Haluza, P., Obdržálek, Š., Matas, J., Lourakis, M., Zabulis, X.: T-less:
732 An rgb-d dataset for 6d pose estimation of texture-less objects. In: Applications
733 of Computer Vision (WACV), 2017 IEEE Winter Conference on, IEEE (2017)
734 880–888
735 40. Borji, A., Izadi, S., Itti, L.: ilab-20m: A large-scale controlled object dataset to
736 investigate deep learning. In: Computer Vision and Pattern Recognition (CVPR),
737 2016 IEEE Conference on, IEEE (2016) 2221–2230
738 41. Lai, K., Bo, L., Ren, X., Fox, D.: A large-scale hierarchical multi-view rgb-d
739 object dataset. In: Robotics and Automation (ICRA), 2011 IEEE International
740 Conference on, IEEE (2011) 1817–1824
741 42. Chang, A.X., Funkhouser, T., Guibas, L., Hanrahan, P., Huang, Q., Li, Z.,
742 Savarese, S., Savva, M., Song, S., Su, H., Xiao, J., Yi, L., Yu, F.: ShapeNet:
743 An Information-Rich 3D Model Repository. Technical Report arXiv:1512.03012
744 [cs.GR], Stanford University — Princeton University — Toyota Technological Institute
745 at Chicago (2015)
746 43. Su, H., Maji, S., Kalogerakis, E., Learned-Miller, E.: Multi-view convolutional
747 neural networks for 3d shape recognition. In: Proceedings of the IEEE international
748 conference on computer vision. (2015) 945–953
749 44. Kirkpatrick, J., Pascanu, R., Rabinowitz, N.C., Veness, J., Desjardins, G., Rusu,
750 A.A., Milan, K., Quan, J., Ramalho, T., Grabska-Barwinska, A., Hassabis, D.,
751 Clopath, C., Kumaran, D., Hadsell, R.: Overcoming catastrophic forgetting in
752 neural networks. CoRR **abs/1612.00796** (2016)
753 45. French, R.M.: Catastrophic forgetting in connectionist networks. Trends in cognitive
754 sciences **3**(4) (1999) 128–135
755 46. Xiang, Y., Choi, W., Lin, Y., Savarese, S.: Data-driven 3d voxel patterns for object
756 category recognition. In: Proceedings of the IEEE Conference on Computer Vision
757 and Pattern Recognition. (2015) 1903–1911
758 47. Bai, S., Bai, X., Zhou, Z., Zhang, Z., Latecki, L.J.: Gift: A real-time and scalable
759 3d shape search engine. In: Computer Vision and Pattern Recognition (CVPR),
760 2016 IEEE Conference on, IEEE (2016) 5023–5032